



A Monte Carlo simulation study of associated liquid crystals

R. BERARDI, M. FEHERVARI and C. ZANNONI*

Dipartimento di Chimica Fisica e Inorganica, Università, Viale Risorgimento 4,
40136 Bologna, Italy

(Received 7 July 1999; accepted 20 July 1999)

We have performed a Monte Carlo simulation study of a system of ellipsoidal particles with *donor-acceptor* sites modelling complementary hydrogen-bonding groups in real molecules. We have considered elongated Gay-Berne particles with terminal interaction sites allowing particles to associate and form dimers. The changes in the phase transitions and in the molecular organization and the interplay between orientational ordering and dimer formation are discussed. Particle *flip* and *dimer* moves have been used to increase the convergency rate of the Monte Carlo (MC) Markov chain.

1. Introduction

A key molecular ingredient for the formation of liquid crystalline phases is the presence of a sufficiently pronounced anisotropy of shape or of some other suitable interaction. This in effect rules out a very large number of potential mesogens that are not sufficiently elongated or 'squashed'. A fascinating possibility, however, is that these would-be mesogens could attach one to the other and dimerize, e.g. through terminal hydrogen bonds, and that the newly formed dimer could then form a liquid crystal. The existence of such proto-mesogenic species that can generate nematic and smectic liquid crystalline phases via recognition induced self-assembly is widely reported in the literature [1–11]. In particular the peculiar rôle played by hydrogen bonding in determining the thermodynamic and structural properties of liquid crystalline materials, that has been known since the early works of Gray and co-workers [1, 2] has recently been addressed by a number of experimental and theoretical investigations [3–18]. The simplest one component systems exhibiting a liquid crystalline phase formed by a dimerizing molecule are probably those based on benzoic acids [1–3]. Two components systems are also well known, and equimolar mixtures of pyridinic p-substituted compounds (often stilbazoles) with benzoic acids [4, 5] or nitrophenols [6] provide typical examples. Ferroelectric [7], cholesteric [8], nematic as well as columnar [12] liquid crystals formed by associated molecules have been produced using the basic idea of complementary building blocks as a guideline. The application of these principles has also led to the investigation of a multitude of other self-assembled

systems [11] like the supramolecular liquid crystalline polymers studied by Lehn and co-workers [13]. Experimental estimates of the fraction of dimerized molecules and a quantitative study of the effect of the hydrogen bond in determining the overall phase structure have recently been put forward [3, 4, 6] analysing, at different temperatures, the characteristic infrared (IR) bands of hydrogen-bonding groups. These studies have confirmed the importance of association between proto-mesogenic molecules combined with strong anisotropic interactions for the formation of liquid crystalline phases.

The theoretical studies of hydrogen-bonding systems comprise several models, mainly based on modifications of hard particle ones, designed to interpret association driven mesogenic behaviour. Starting from Onsager's theory [14], Sear and Jackson [15] and Veytsman [16] have developed mean field theories of dimerizing fluids of spherocylinders [15] and rod-like [16] hard particles with attractive sites at one end. These models exhibit phases where the dimerized *end-to-end* particles are aligned, like proto-mesogen carboxylic acids [1–3] and represent a valuable contribution to the study of thermodynamic effects of associating liquids. Computer simulations of model liquid crystalline phases formed by hydrogen-bonding hard particles have also been performed [17, 18]. The comparison between theoretical predictions [15] and Monte Carlo computer simulation results [18] of associating spherocylinders with *length-to-breadth* ratio $k = 3$ demonstrates how a non-mesogenic fluid can undergo a phase transition from isotropic to nematic as long as particles are capable of dimerizing to form a sufficiently anisotropic particle. While hard particle based models are certainly very relevant, they suffer for a study of thermotropics like the one of interest here, from the fact that the only temperature dependence in

* Author for correspondence. e-mail: vz3bod7a@sirio.cineca.it

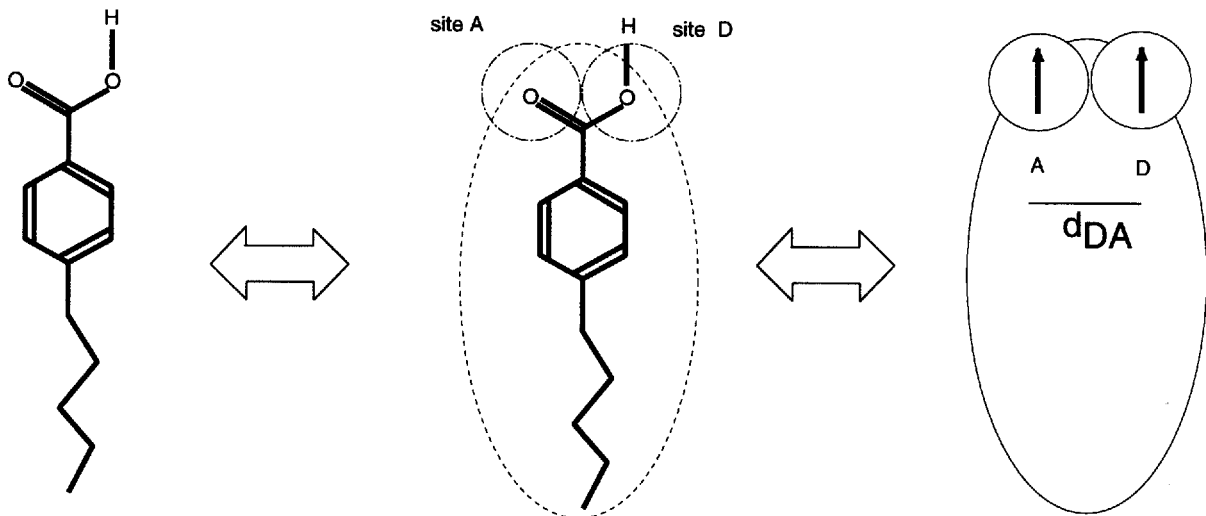


Figure 1. Schematic representation of a carboxylic acid as a *donor-acceptor* system embedded in an ellipsoidal polarizability centre.

the system comes exclusively from the hydrogen bond interactions. This is at a significant difference from a real thermotropic where hydrogen-bonding interactions will only represent a fraction of the total interaction energy.

In this work we present the results of Monte Carlo computer simulations of a system with anisotropic attractive and repulsive interactions formed by short rod-like Gay-Berne particles of *length-to-breadth* ratio $k = 2$ and with hydrogen-bonding-like sites at one end. We shall consider hydrogen bonds of two different strengths and examine the interplay of dimerization with the formation of order and the nematic-isotropic transition.

2. Model

We have studied a model fluid formed by attractive-repulsive Gay-Berne (GB) [19] ellipsoidal particles with two terminal embedded sites, which aim to model the interaction mechanism of hydrogen-bonding groups. In figure 1 we show an example of the molecule we have in mind: a simple two-site system for a carboxylic group with the oxygen and the oxydriol respectively modelled with an H *acceptor* (A) and an H *donor* (D) sites at distance d_{DA} . We assume the pair interaction energy of two such molecules to be the sum of three contributions

$$U = U_{GB}(1, 2) + U_{DA}(1, 2) + U_{DA}(2, 1), \quad (1)$$

namely, the GB energy, the interaction of *donor* site in particle 1 with *acceptor* site in molecule 2, and vice versa. The uniaxial Gay-Berne potential [19] is an anisotropic Lennard-Jones potential

$$\begin{aligned} U_{GB}(1, 2) &\equiv U_{GB}(\mathbf{r}_{12}, \hat{\mathbf{u}}_1, \hat{\mathbf{u}}_2) \\ &= 4\epsilon_0 \epsilon(\hat{\mathbf{r}}_{12}, \hat{\mathbf{u}}_1, \hat{\mathbf{u}}_2) \\ &\quad \times \left\{ \left(\frac{\sigma_s}{r_{12} - \sigma(\hat{\mathbf{r}}_{12}, \hat{\mathbf{u}}_1, \hat{\mathbf{u}}_2) + \sigma_s} \right)^{12} \right. \\ &\quad \left. - \left(\frac{\sigma_s}{r_{12} - \sigma(\hat{\mathbf{r}}_{12}, \hat{\mathbf{u}}_1, \hat{\mathbf{u}}_2) + \sigma_s} \right)^6 \right\}, \quad (2) \end{aligned}$$

where the unit vectors $\hat{\mathbf{u}}_1$ and $\hat{\mathbf{u}}_2$ define the molecular orientations of the monomers, $\mathbf{r}_{12} = \mathbf{r}_2 - \mathbf{r}_1 \equiv r_{12}\hat{\mathbf{r}}_{12}$ is the intermolecular vector of length r_{12} and orientation $\hat{\mathbf{r}}_{12}$. The molecular units for energies and distances are taken to be ϵ_0 and σ_s . The energy anisotropy $\epsilon(\hat{\mathbf{r}}_{12}, \hat{\mathbf{u}}_1, \hat{\mathbf{u}}_2)$ and shape anisotropy $\sigma(\hat{\mathbf{r}}_{12}, \hat{\mathbf{u}}_1, \hat{\mathbf{u}}_2)$ are defined as in [19, 20] in terms of particle dimensions σ_s, σ_e , potential well depths ϵ_s, ϵ_e and model exponents μ, ν .

To model a hydrogen-bonding-like interaction and its peculiar features, namely directionality and strength, we propose an anisotropic *donor-acceptor* (DA) potential where the interaction of a *donor* site in molecule 1 with an *acceptor* site in molecule 2 is written as

$$\begin{aligned} U_{DA}(1, 2) &\equiv U_{DA}(\mathbf{r}_{DA}, \hat{\mathbf{u}}_D, \hat{\mathbf{u}}_A) \\ &= 15\epsilon_0 \epsilon_{DA}(\hat{\mathbf{r}}_{DA}, \hat{\mathbf{u}}_D, \hat{\mathbf{u}}_A) \\ &\quad \times \left\{ \left(\frac{\sigma_{DA}}{r_{DA}} \right)^{12} - \left(\frac{\sigma_{DA}}{r_{DA}} \right)^{10} \right\}, \quad (3) \end{aligned}$$

where σ_{DA} is the contact distance for the DA interaction (i.e. $U_{DA} = 0$ for $r_{DA} = \sigma_{DA}$). The unit vectors $\hat{\mathbf{u}}_D, \hat{\mathbf{u}}_A$ specify the orientations of *donor* and *acceptor* sites and $\mathbf{r}_{DA} \equiv \mathbf{r}_A - \mathbf{r}_D \equiv r_{DA}\hat{\mathbf{r}}_{DA}$ is the inter-site vector (see

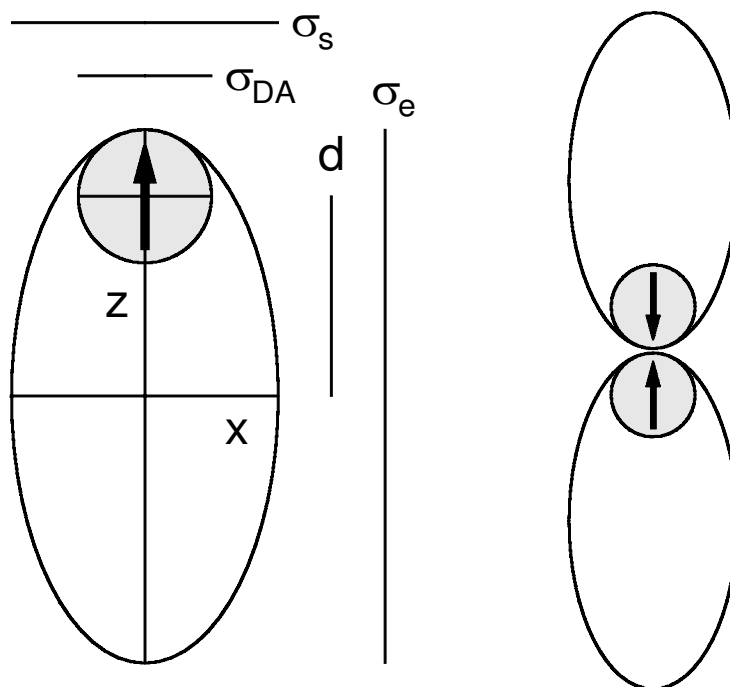


Figure 2. Schematic representations of a uniaxial Gay-Berne particle (left) and an associated pair (right). The prolate ellipsoid has axes σ_e and σ_s with embedded *donor* (D) and *acceptor* (A) sites positioned along the principal axis at distance d from the centre. The overlapped D and A sites ($d_{DA} = 0$) have diameter σ_{DA} and orientation $\hat{\mathbf{u}}_D, \hat{\mathbf{u}}_A$ (shown as a black arrow) parallel to \mathbf{z} .

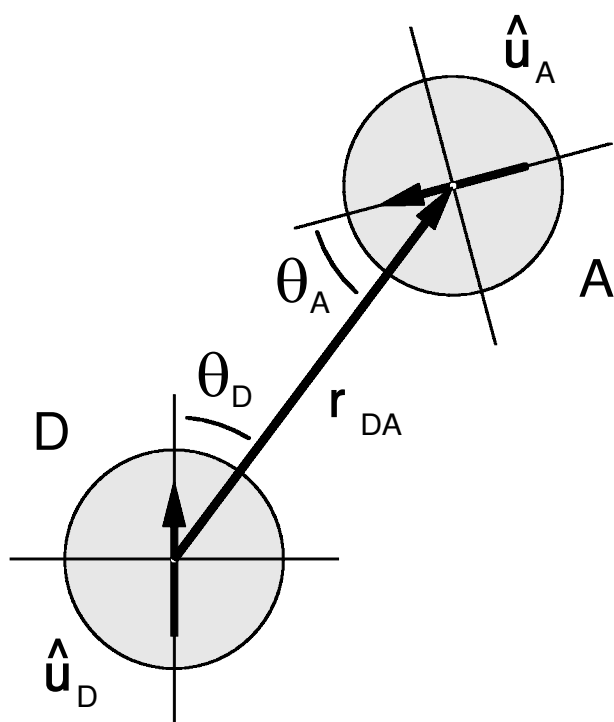


Figure 3. Interaction scheme of a *donor* (D) and *acceptor* (A) sites of orientation $\hat{\mathbf{u}}_D, \hat{\mathbf{u}}_A$ and inter-site vector $\mathbf{r}_{DA} \equiv \mathbf{r}_A - \mathbf{r}_D = r_{DA}\hat{\mathbf{r}}_{DA}$.

figures 2 and 3). The r^{-10} distance dependence of the attractive branch is consistent with the expected short range of the hydrogen-bonding energy [21–24].

The interaction anisotropy $\epsilon_{DA}(\hat{\mathbf{r}}_{DA}, \hat{\mathbf{u}}_D, \hat{\mathbf{u}}_A)$ defines how the DA energy surface depends on the two complementary sites [25–27]. We take

$$\epsilon_{DA}(\hat{\mathbf{r}}_{DA}, \hat{\mathbf{u}}_D, \hat{\mathbf{u}}_A) = \frac{\epsilon_{DA}^+}{\epsilon_0} \left\{ \left(\frac{1 + \hat{\mathbf{u}}_D \cdot \hat{\mathbf{r}}_{DA}}{2} \right) \left(\frac{1 - \hat{\mathbf{u}}_A \cdot \hat{\mathbf{r}}_{DA}}{2} \right) \right\}^\xi, \quad (4)$$

where ϵ_{DA}^+ is the well depth for the DA interaction, while the exponent ξ plays the role of an angular sensitivity which determines the amplitude of the DA well.

The configuration that maximizes the interaction is that with sites D and A aligned parallel and anti-parallel to the inter-site vector (i.e. $\hat{\mathbf{u}}_D \cdot \hat{\mathbf{r}}_{DA} = 1$ and $\hat{\mathbf{u}}_A \cdot \hat{\mathbf{r}}_{DA} = -1$) and at distance $r_{DA}^+ = (6/5)^{1/2} \sigma_{DA}$ corresponding to an energy $U_{DA}^+ = -5^6 / (2 \times 6^5) \epsilon_{DA}^+ \approx -\epsilon_{DA}^+$ (see figure 2, right).

We assume the *donor* and *acceptor* sites to be placed at a certain fixed distance d_{DA} and, for the present work, to be placed in near terminal position along the monomer axis at a distance d from the centre. Since d_{DA} is expected to be relatively small compared to the molecular dimension in this paper, we make the further

simplification that $d_{\text{DA}} = 0$, i.e. that the *donor* and *acceptor* sites can be considered superimposed from the point of view of modelling their effect (see figure 2).

3. Monte Carlo methodology

We intend to study our model using Monte Carlo simulations. However, the standard Metropolis algorithm [28], which performs *monomer* moves, is not efficient in equilibrating the type of associating systems we are dealing with, especially at low temperatures T^* , where the number of dimers could outnumber that of non-associated molecules. In fact, associated particles are more likely to move as a whole *cluster* (here a dimer), rather than individually. To improve the efficiency of the MC Markov chain in sampling the configuration space we have thus found it essential to implement the so-called *cluster* and *cluster-volume* moves [29–32] particularly in the form put forward by Chandler and co-workers [29] and Orkoulas and Panagiotopoulos [30]. The theoretical framework behind the Monte Carlo *cluster* moves, or more generally, a biased sampling for the MC Markov chain, has already been described in the literature [31, 33] and here we only summarize what is essential for the treatment. We start from the detailed balance constraint for a *cluster* move, which can be written as

$$w_{\text{B}(O)} p_{\text{sel}(c_o)} \pi(c_o \rightarrow c_n) p_{\text{acc}(c_o \rightarrow c_n)} \\ = w_{\text{B}(N)} p_{\text{sel}(c_n)} \pi(c_n \rightarrow c_o) p_{\text{acc}(c_n \rightarrow c_o)}, \quad (5)$$

where the labels c_o , c_n denote a *cluster* of particles in the *old* (o) and *new* (n) configurations. $w_{\text{B}(O)}$ and $w_{\text{B}(N)}$ are Boltzmann weights, $p_{\text{sel}(c_o)}$ and $p_{\text{sel}(c_n)}$ are the probabilities of selecting the *cluster* in the *old* and *new* configurations, $\pi(c_o \rightarrow c_n)$ and $\pi(c_n \rightarrow c_o)$ are the transition probabilities, $p_{\text{acc}(c_o \rightarrow c_n)}$ and $p_{\text{acc}(c_n \rightarrow c_o)}$ are the acceptance probabilities for the *forward* and *backward* MC moves. Using a symmetric jump rule $\pi(c_o \rightarrow c_n) = \pi(c_n \rightarrow c_o)$ the acceptance criterion for the *forward* MC *cluster* move becomes

$$p_{\text{acc}(c_o \rightarrow c_n)} = \min \left[1, \frac{w_{\text{B}(N)} p_{\text{sel}(c_n)}}{w_{\text{B}(O)} p_{\text{sel}(c_o)}} \right]. \quad (6)$$

The actual computation of the *cluster* selection probabilities $p_{\text{sel}(c_n)}$, $p_{\text{sel}(c_o)}$ could be extremely time consuming using a *probabilistic* algorithm [29–32] since this would involve scanning the whole sample for estimating the probability that the selected particles actually do belong to a *cluster* and the remaining ones do not. Furthermore, an algorithm based on the evaluation of a specific interaction which is almost zero over the ensemble of pair configurations $\{\mathbf{r}_{12}, \hat{\mathbf{u}}_1, \hat{\mathbf{u}}_2\}$ except for a small subset, would give the ratio $p_{\text{sel}(c_n)}/p_{\text{sel}(c_o)}$ often close to unity. In this case the so-called *deterministic*

algorithm described in [29, 30] can be computationally more efficient than the *probabilistic* one described so far. Using this approach, the selection probability for a group of molecules is either 0 (non-associated state) or 1 (associated state) and the selection probability of an existing *cluster* cannot be altered as a result of a *cluster* move. The distribution of bonded and non-bonded particles is then fixed and the acceptance rule becomes

$$p_{\text{acc}(c_o \rightarrow c_n)} = \min \left[1, \frac{w_{\text{B}(N)}}{w_{\text{B}(O)}} \right], \quad (7)$$

which is the standard Metropolis rule [28]. In this case, a suitable algorithm for the creation and destruction of the existing *clusters* has to be implemented separately [29–32] and the MC simulation is performed randomly alternating the two evolution schemes.

For our MC simulations we have chosen to use a *deterministic* selection algorithm based on the magnitude of the DA interaction. Furthermore, since our parametrization for the DA pair interaction makes the formation of trimers and higher n -mers extremely unlikely the algorithm performs *cluster* moves of just one pair of associated particles. The schematic description of the *deterministic* algorithm we have used to perform these *dimer* moves is as follows.

- (a) Select a particle i at random.
- (b) Scan all N_c neighbours of i within a suitable cut-off radius r_c . Two GB particles are considered associated if $U_{\text{DA}} = U_{\text{DA}}(1, 2) + U_{\text{DA}}(2, 1) \leq -\epsilon_0$. Select the particle j whose U_{DA} interaction is the most favourable and define in the *old* configuration the (i, j) dimer (*cluster*) just found.
- (c) Generate a random translation or rotation for the *dimer* (i, j) .
- (d) After the attempted move, scan again all neighbouring particles N_c of i in the *new* configuration and identify particle j' using again criterion (b).
- (e) If $j \neq j'$ the *dimers* in the *old* and *new* configurations are not identical, then the move is rejected since it violates the microscopic reversibility hypothesis.
- (f) If $j \equiv j'$ the *dimer* is preserved and the move is further tested for acceptance using the rule in equation (7).

Using this prescription the ratio $p_{\text{sel}(c_n)}/p_{\text{sel}(c_o)} = 1$ for each *dimer* move. We have chosen to perform disjoint translation and rotation *dimer* moves to improve the efficiency of configuration space sampling for a given overall acceptance ratio since it is then possible to use larger sampling ranges. To ensure the necessary creation and destruction of the existing dimers outside the *deter-*

ministic evolution we have chosen to randomly alternate *dimer* and *monomer* moves with a 50% probability each.

The conventional *volume* move was realized allowing each box side to be adjusted independently. A typical volume move consists of a random selection of a box side, followed by a random sampling of a side displacement. The *volume* move is accepted or rejected with a probability given by the *NPT* criterion [33, 34]

$$p_{\text{acc}}(\mathbf{o} \rightarrow \mathbf{n}) = \min \{1, \exp[-\beta(\Delta U + P\Delta V) + N\Delta \ln V]\}.$$

Using this prescription the volume V is linearly sampled. A *cluster-volume* move preserving the relative configuration of associated molecules is equivalent to a sequence of two independent moves. The first one is a standard *NPT* volume move, i.e. an attempted expansion (or contraction) of one side of the simulation box whose detailed balance is

$$w_{NPT}(V_o, \{c_o\}) \pi(V_o \rightarrow V_n) p_{\text{acc}}(V_o \rightarrow V_n) \\ = w_{NPT}(V_n, \{c_n\}) \pi(V_n \rightarrow V_o) p_{\text{acc}}(V_n \rightarrow V_o), \quad (8)$$

where $w_{NPT}(V_o, \{c_o\})$ and $w_{NPT}(V_n, \{c_n\})$ are the *NPT* statistical weights for the configurations with volumes V_o, V_n and $\{c_n\}, \{c_o\}$ are the collections of all *clusters* with *old* and *new* relative inter-*cluster* distances. The second is a *multi-particle* move which attempts to restore the intermolecular distances within all *clusters* to the values they had before the volume move

$$w_{NPT}(V_n, \{c_n\}) \prod_{\{c_n\}} p_{\text{sel}}(c_n) \pi(c_n \rightarrow c_o) p_{\text{acc}}(c_n \rightarrow c_o) \\ = w_{NPT}(V_n, \{c_o\}) \prod_{\{c_o\}} p_{\text{sel}}(c_o) \pi(c_o \rightarrow c_n) p_{\text{acc}}(c_o \rightarrow c_n). \quad (9)$$

We use again symmetrical transition distributions and we define the total conditional acceptance probability for the *cluster-volume* move as

$$p_{\text{acc}}(V_o \rightarrow V_n | \{c_o\}) = p_{\text{acc}}(V_o \rightarrow V_n) \prod_{\{c_n\}} p_{\text{acc}}(c_n \rightarrow c_o). \quad (10)$$

For our *deterministic dimer* selection algorithm we have

$$p_{\text{acc}}(V_o \rightarrow V_n | \{c_o\}) = \min \left[1, \frac{w_{NPT}(V_n, \{c_o\})}{w_{NPT}(V_o, \{c_o\})} \right]. \quad (11)$$

which is the standard isobaric–isothermal criterion [33, 34]

The switching from conventional *monomer* to *dimer* MC evolution was automatically performed during the simulation runs whenever the instantaneous value of the *donor–acceptor* energy per particle $U_{\text{DA}}^* \leq -1$. The sampling of phase space has been performed using sym-

metric sampling intervals for particle translations, rotations and box sides. The sampling widths have been tuned in order to obtain, from case to case, an overall move acceptance ratio in the range [0.2, 0.4]. In addition, it was useful to replace part of the MC *rotation–translation monomer* moves with the so-called particle *flip* moves. They consist in an inversion of the $\hat{\mathbf{u}}_i$ vector and thus in an exchange of molecular head with tail [18, 35, 36]. In practice, *flip* moves were attempted with a frequency $p_{\text{flip}} = 0.2$ during the MC evolution.

4. Simulations and results

We have considered various model systems, each formed by $N = 512$ prolate Gay–Berne (GB) [19] particles with shape anisotropy $\kappa \equiv \sigma_e/\sigma_s = 2$, interaction anisotropy $\kappa' \equiv \epsilon_s/\epsilon_e = 3$, where $\epsilon_s^* \equiv \epsilon_s/\epsilon_0 = 1.5$, $\epsilon_e^* \equiv \epsilon_e/\epsilon_0 = 0.5$, and model exponents $\mu = 1$, $\nu = 3$ [37]. The *donor* and *acceptor* sites of dimension $\sigma_{\text{DA}}^* \equiv \sigma_{\text{DA}}/\sigma_s = 0.5$ have been placed at distance $d^* \equiv d/\sigma_s = 0.75$ from the molecular centre along the principal axis (see figure 2). Using these parameters the overall shape given by the repulsive part of the potential energy surface remains nearly ellipsoidal. In figure 4 we show the overall interaction energy surface for two associated pairs in a *side-by-side* configuration.

We have treated on one hand non-associating particles, and on the other molecules with two rather different values of the *donor–acceptor* energy strength, namely $\epsilon_{\text{DA}}^+/\epsilon_0 = 5$ (system A_1) and $\epsilon_{\text{DA}}^+/\epsilon_0 = 10$ (system A_2). If we assume the energy scale to be $\epsilon_0 = 0.831 \text{ kJ mol}^{-1}$ this would correspond to a hydrogen bond strength of roughly 4 and 8 kJ mol^{-1} all falling in the realm of ‘*weak hydrogen bonds*’ according to current classifications [38]. For both systems the angular sensitivity exponent was $\xi = 33$. In figures 5 and 6 we report the relevant energy profiles for the interaction of *donor* and *acceptor* sites using the parametrization described so far. In particular, to examine how the value of ϵ_{DA}^+ actually affects the association properties, we show in figure 5 the distance dependence of the DA interaction for two perfectly aligned monomers approaching *head on*. We see that the DA interaction for system A_1 is almost twice the GB energy for the *side-by-side* configuration, while for system A_2 it is almost four times stronger. We thus refer to A_1 and A_2 as weakly and strongly associating systems.

We have performed MC simulations in the isobaric–isothermal ensemble (*NPT*) [33, 34]. A cut-off radius of $r_c^* \equiv r_c/\sigma_s = 2.8$ has been employed in the MC evolution for the computation of the pair energy U^* (figure 5). In figure 6 we describe the influence of the approach angle θ_D on the U_{DA}^* energy ($\theta_A = 0$ and r_{DA} constant) for *donor* and *acceptor* sites in the configuration shown in figure 3. We see that using an angular sensitivity $\xi = 33$

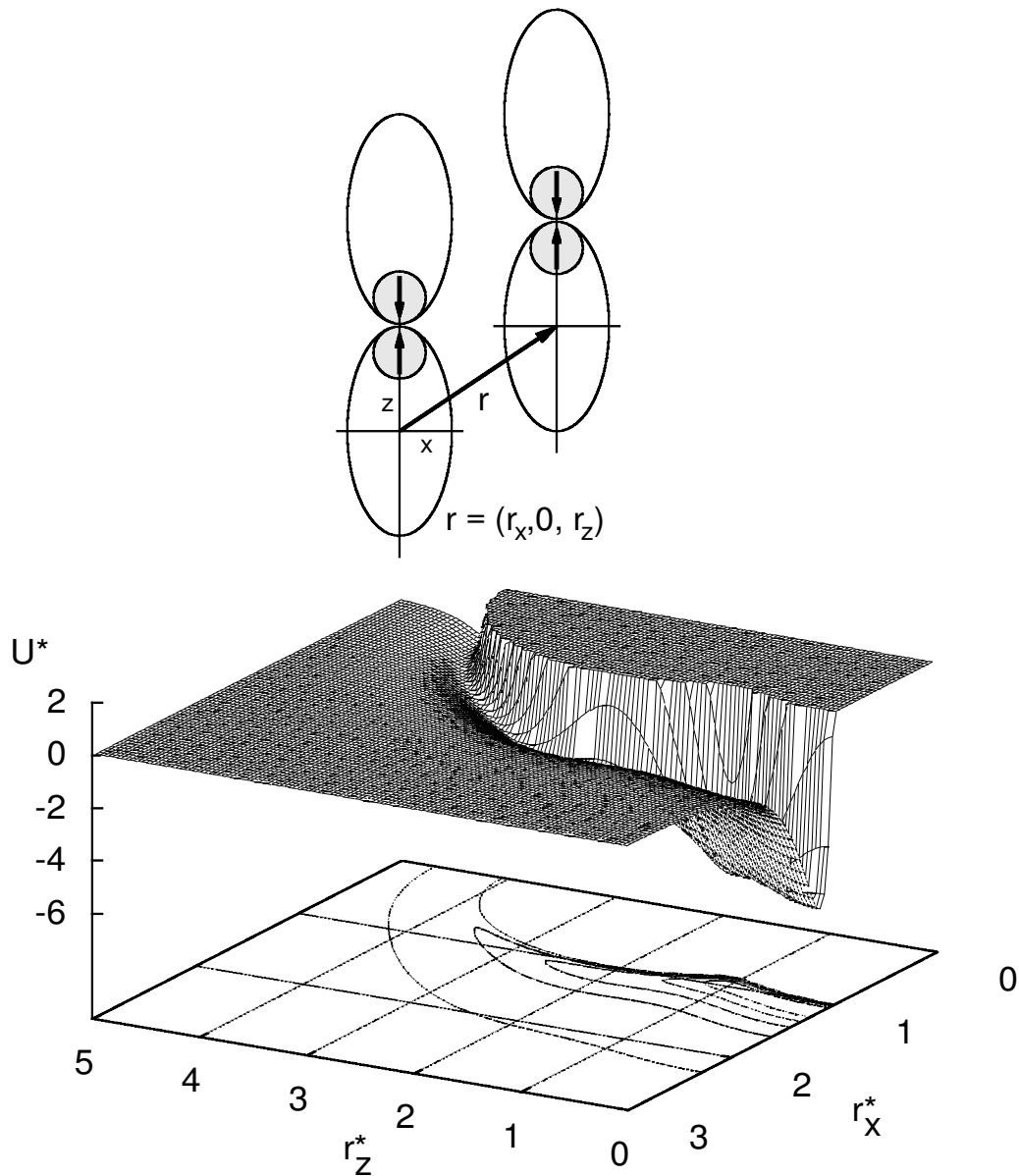


Figure 4. Energy surface for two parallel associated pairs in a *side-by-side* configuration.

the DA energy rapidly decreases with the *donor* and *acceptor* sites misalignment angle θ_D . In practice, a cut-off angle $\theta_c = 30.68^\circ$ for θ_D , θ_A angle has been used for the computation of the U_{DA}^* interaction during the MC evolution (figure 6). Using this parametrization for the pair interaction the simultaneous association of three or more particles is extremely unfavourable from an energetic point of view and only dimerization is practically accessible at the temperatures and pressure we have studied, avoiding the formation of catamers or branched structures.

The fluid MC sample has been simulated in a box of sides L_x , L_y and L_z at constant scaled internal

pressure $P^* \equiv P\sigma_s^3/\epsilon_0 = 3$ and with periodic boundary conditions. The volume of the simulation box is $V^* \equiv V/\sigma_s^3 = L_x L_y L_z/\sigma_s^3$ and the number density is thus $\rho^* \equiv \sigma_s^3 \rho = \sigma_s^3 N/V$. The average pressure was maintained constant during the simulation run using the conventional isobaric-isothermal algorithm [33, 34] with the changes described in the previous section. Random *volume* moves were attempted during the MC evolution with a frequency inversely proportional to the number of particles, $p_{\text{box}} = 0.02/N$, i.e. on average every 50 cycles, a cycle being a sequence of N attempted *monomer* (or *dimer*) moves.

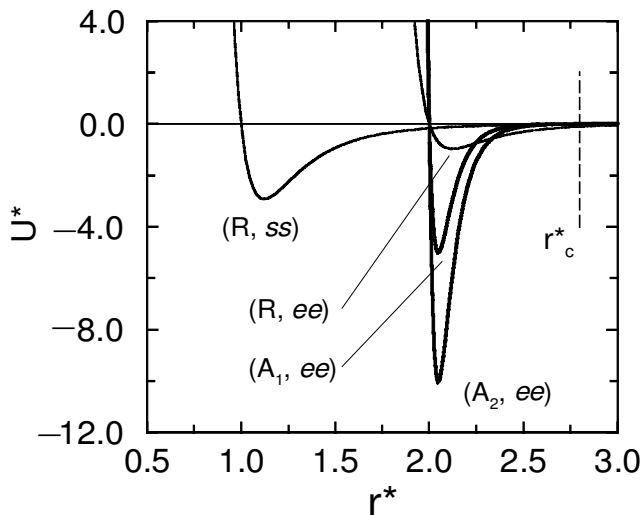


Figure 5. Distance dependence of the donor-acceptor pair energy U^*_{DA} for $\epsilon^+_{DA}/\epsilon_0 = 5$ (curve A₁, ee) and $\epsilon^+_{DA}/\epsilon_0 = 10$ (curve A₂, ee) for the associated end-to-end configuration of figure 2. The Gay-Berne energy U^*_{GB} for the end-to-end (curve R, ee) and side-by-side (curve R, ss) configurations are reported for comparison. The radial cut-off $r^*_c \equiv r_c/\sigma_s = 2.8$ employed for the total interaction $U^* = U^*_{GB} + U^*_{DA}$ is marked with a dashed line.

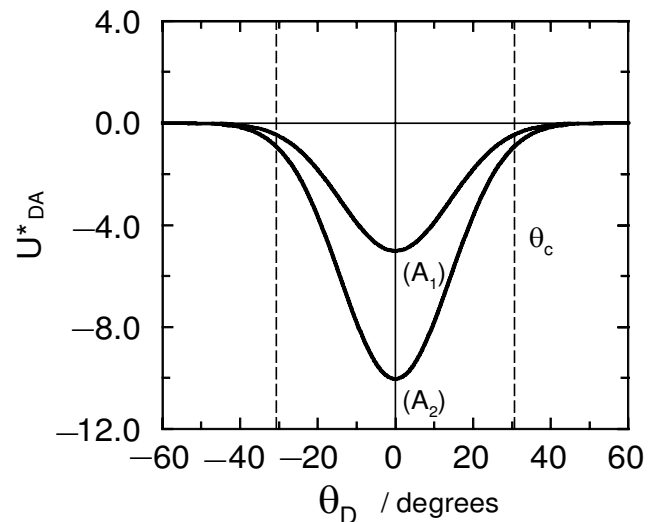


Figure 6. The angular dependence of the U^*_{DA} energy profile with $\epsilon^+_{DA}/\epsilon_0 = 5$ (curve A₁) and $\epsilon^+_{DA}/\epsilon_0 = 10$ (curve A₂) for a donor-acceptor pair at a constant distance $r_{DA} = r^+_{DA} \equiv (6/5)^{1/2} \sigma_{DA}$ and angular sensitivity exponent $\xi = 33$. The donor approach angle θ_D (see figure 3) is $\hat{\mathbf{u}}_D \cdot \hat{\mathbf{r}}_{DA} = \cos \theta_D$, while the relative orientation of the acceptor site is constrained to $\hat{\mathbf{u}}_A \cdot \hat{\mathbf{r}}_{DA} = -\cos \theta_A = -1$. The angular cut-offs $|\cos \theta_c| = 0.86$ (angles θ_D, θ_A) for the U^*_{DA} interaction are marked with the dashed lines.

Table 1. The average enthalpy $\langle H^* \rangle$, Gay-Berne $\langle U^*_{GB} \rangle$ and donor-acceptor $\langle U^*_{DA} \rangle$ energies per molecule, the number density $\langle \rho^* \rangle$, the concentration of dimers $\langle bp \rangle \%$ and the second rank orientational order parameter $\langle P_2 \rangle$ for bulk systems of $N = 512$ non-bonding ($\epsilon^+_{DA}/\epsilon_0 = 0$, system R), moderately associating ($\epsilon^+_{DA}/\epsilon_0 = 5$, system A₁) and strongly associating ($\epsilon^+_{DA}/\epsilon_0 = 10$, system A₂) particles at a dimensionless pressure $P^* = 3$. Root mean square errors for the average properties are ± 1 on the last digit shown.

T^*	System R				System A ₁						System A ₂					
	$\langle \rho^* \rangle$	$\langle H^* \rangle$	$\langle U^*_{GB} \rangle$	$\langle P_2 \rangle$	$\langle \rho^* \rangle$	$\langle H^* \rangle$	$\langle U^*_{GB} \rangle$	$\langle U^*_{DA} \rangle$	$\langle bp \rangle \%$	$\langle P_2 \rangle$	$\langle \rho^* \rangle$	$\langle H^* \rangle$	$\langle U^*_{GB} \rangle$	$\langle U^*_{DA} \rangle$	$\langle bp \rangle \%$	$\langle P_2 \rangle$
1.00	0.514	-5.37	-11.58	0.94	-	-	-	-	-	-	-	-	-	-	-	-
1.05	0.511	-5.18	-11.43	0.93	-	-	-	-	-	-	-	-	-	-	-	-
1.10	0.477	-2.50	-9.32	0.84	0.516	-7.79	-11.32	-2.83	67.6	0.96	-	-	-	-	-	-
1.15	0.471	-2.09	-9.01	0.82	0.514	-7.35	-11.16	-2.60	61.7	0.96	-	-	-	-	-	-
1.20	0.465	-1.67	-8.69	0.79	0.468	-2.58	-8.92	-0.55	12.5	0.82	-	-	-	-	-	-
1.25	0.457	-1.21	-8.31	0.74	0.462	-1.93	-8.63	-0.41	9.1	0.79	-	-	-	-	-	-
1.30	0.451	-0.95	-8.04	0.72	0.455	-1.42	-8.26	-0.29	6.3	0.75	-	-	-	-	-	-
1.35	0.442	-0.22	-7.51	0.63	0.446	-0.71	-7.78	-0.21	4.2	0.69	-	-	-	-	-	-
1.40	-	-	-	-	0.437	-0.07	-7.27	-0.13	2.6	0.59	0.508	-12.50	-11.19	-7.85	93.7	0.98
1.45	0.420	1.41	-6.13	0.15	-	-	-	-	-	-	0.503	-11.92	-10.95	-7.65	91.6	0.98
1.50	0.414	1.79	-5.90	0.10	0.416	1.73	-5.98	-0.04	0.7	0.12	0.456	-8.35	-8.87	-6.51	78.3	0.89
1.55	0.409	1.89	-5.77	0.09	0.410	1.91	-5.79	-0.03	0.5	0.10	0.446	-7.46	-8.46	-5.97	71.4	0.86
1.60	0.405	2.09	-5.67	0.08	0.406	2.18	-5.68	-0.02	0.4	0.09	0.441	-6.11	-8.15	-5.34	64.3	0.83
1.65	0.401	2.37	-5.54	0.08	0.401	2.26	-5.54	-0.02	0.3	0.08	0.431	-4.86	-7.64	-4.56	54.8	0.78
1.70	0.396	2.47	-5.42	0.07	0.398	2.56	-5.45	-0.02	0.3	0.07	0.425	-3.10	-7.18	-3.73	45.1	0.68
1.75	0.394	2.72	-5.34	0.07	0.394	2.66	-5.34	-0.02	0.3	0.07	-	-	-	-	-	-
1.80	0.390	2.90	-5.23	0.06	0.389	2.89	-5.22	-0.01	0.2	0.07	0.393	-0.01	-5.58	-2.30	27.0	0.21
1.85	0.385	3.00	-5.12	0.06	0.384	2.94	-5.14	-0.01	0.2	0.07	0.389	2.06	-5.33	-1.65	19.4	0.10
1.90	0.381	3.08	-5.03	0.06	0.382	3.13	-5.06	-0.01	0.2	0.06	0.383	2.58	-5.10	-0.53	6.2	0.06
1.95	0.378	3.30	-4.95	0.06	0.380	3.23	-4.96	-0.01	0.2	0.06	0.382	2.90	-5.04	-0.47	5.5	0.06
2.00	0.376	3.48	-4.89	0.06	0.376	3.54	-4.88	-0.01	0.1	0.06	0.376	3.08	-4.91	-0.36	4.1	0.06

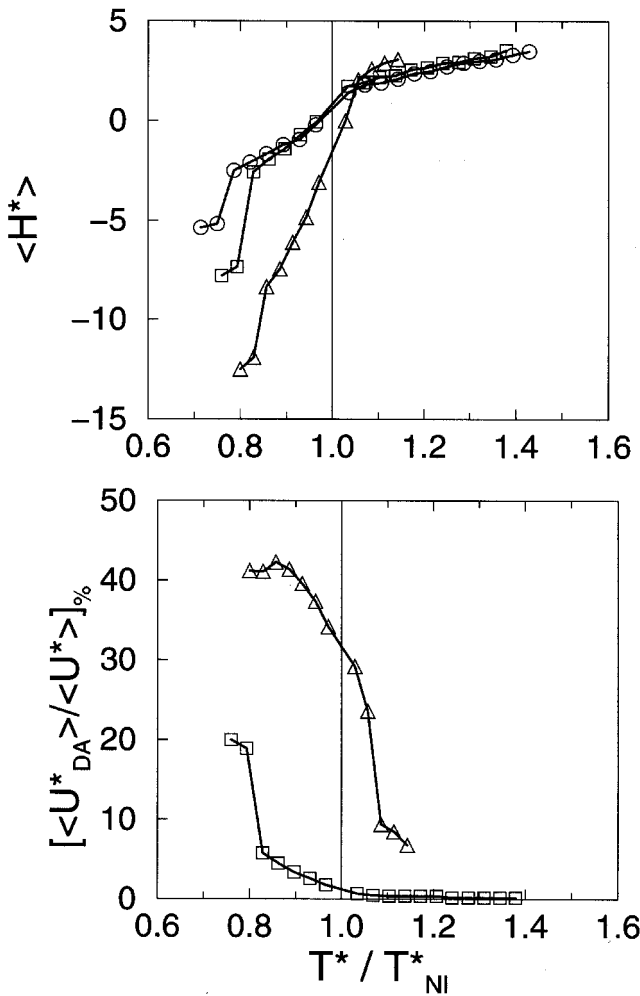


Figure 7. The average enthalpy per molecule $\langle H^* \rangle$ (top plate) and the percentage of *donor-acceptor* energy $[\langle U_{DA}^* \rangle / \langle U^* \rangle]_{\%}$ (bottom plate) for the reference (R, \circ), weakly associating (A₁, \square) and strongly associating (A₂, \triangle) systems. The temperature is scaled with respect to the nematic-isotropic transition $T_{NI}^* \approx 1.45$ for system A₁ and $T_{NI}^* \approx 1.75$ for system A₂.

To provide a reference state for the associated systems, we have simulated first a fluid of purely Gay-Berne particles with the same GB parametrization (and particularly *length-to-breadth* ratio $k = 2$) but without associating capability (system R). We have performed a cooling down sequence starting from dimensionless temperature $T^* = k_B T / \epsilon_0 = 2$ to $T^* = 1$. The reference system R shows isotropic (I), nematic (N) and a smectic (S) phase with $T_{NI}^* \approx 1.40$ and $T_{SN}^* \approx 1.05$. It is interesting to see that even for this low elongation ratio κ , ordered phases are formed, albeit at a very low temperature compared to $T_{NI}^* \approx 2.4$, which we have found for the more usual *length-to-breadth* ratio $\kappa = 3$ for a series of runs performed at the same $P^* = 3$.

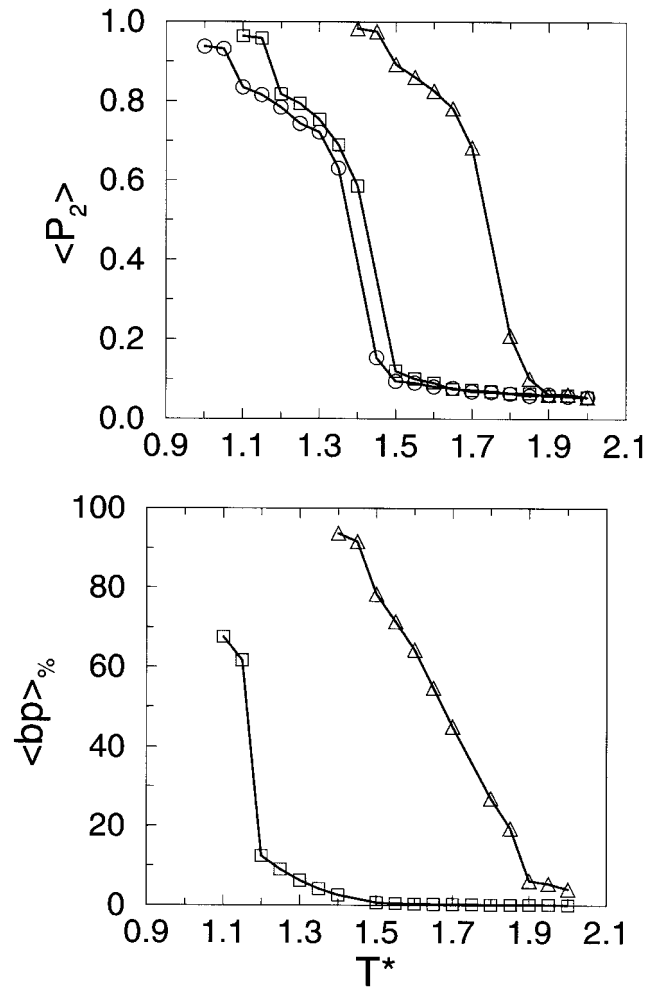


Figure 8. Second rank orientational order parameter $\langle P_2 \rangle$ (top plate) and percentage of bonded particles $\langle bp \rangle_{\%}$ (bottom plate) for systems R (\circ), A₁ (\square) and A₂ (\triangle).

We have then performed two separate sets of simulations for the weakly and strongly associating systems, A₁ and A₂, again starting from the isotropic phase at $T^* = 2$ (densities $\rho^* = 0.376$) and cooling down to $T^* = 1.1$ (system A₁, $\rho^* = 0.516$) and $T^* = 1.4$ (system A₂, $\rho^* = 0.508$). Within these temperature ranges, the associating systems A₁ and A₂ undergo first an isotropic-nematic transition followed by a second phase transition to an extremely ordered phase. In table 1 we show the average enthalpy $\langle H^* \rangle = (\langle U \rangle + P \langle V \rangle) / \epsilon_0$, the Gay-Berne $\langle U_{GB}^* \rangle \equiv \langle U_{GB} \rangle / \epsilon_0$, and *donor-acceptor* $\langle U_{DA}^* \rangle \equiv \langle U_{DA}(1,2) + U_{DA}(2,1) \rangle / \epsilon_0$ energies, the density ρ^* , the percentage of bonded particles, i.e. concentration of dimers, $\langle bp \rangle_{\%}$ and the second rank orientational order parameter $\langle P_2 \rangle$ for the three systems studied. The corresponding plots of some of these observables are given in figures 7 and 8.

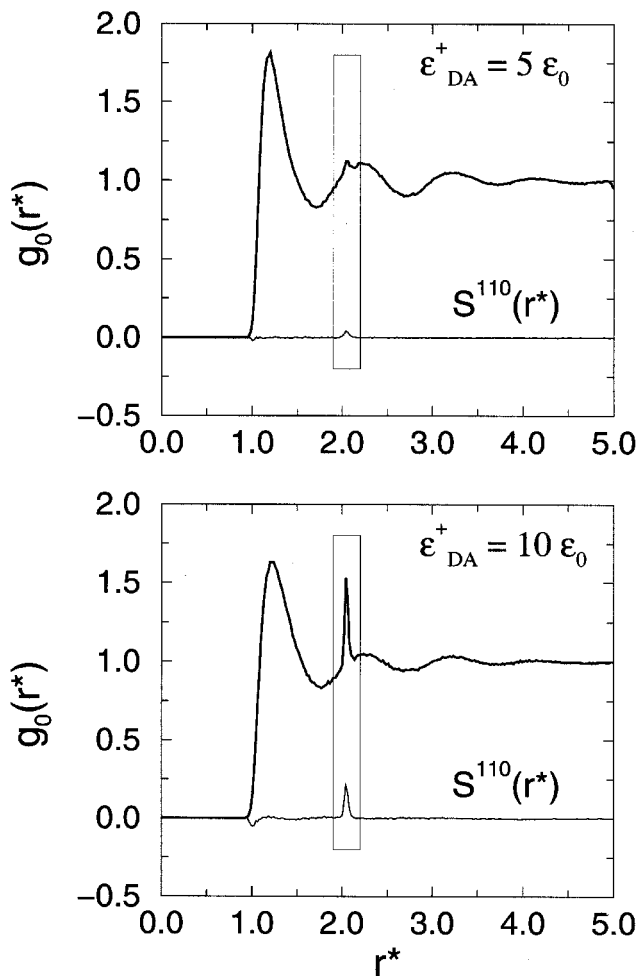


Figure 9. The radial distribution function $g_0(r^*)$ (thick line) and the rotational invariant $S^{110}(r^*)$ (thin line) for system A_1 at $T^* = 1.25$ (top plate, $\langle P_2 \rangle = 0.79$) and system A_2 at $T^* = 1.65$ (bottom plate, $\langle P_2 \rangle = 0.78$). The frames enclose the portion of the histograms centred around the intermolecular separation $r^* \equiv r/\sigma_s \approx 2$ corresponding to associated particles (cf. figure 2).

The analysis of these data shows two different temperature behaviours for the association process and the spontaneous formation of orientational order. Both in systems A_1 and A_2 , the two processes reinforce each other: thus association promotes the particle alignment and vice versa. However, the magnitude of mutual coupling and pre-transitional effects is different in the two cases that we now consider in turn, starting from the weakly associating one.

Comparing system A_1 (low bonding energy, $\epsilon_{\text{DA}}^+/\epsilon_0 = 5$) with the reference system, we see that the association shifts the N–I transition to a slightly higher temperature ($T_{\text{NI}}^* \approx 1.45$) and that the order parameter inside the nematic phase becomes slightly higher. Nonetheless, in the isotropic and nematic phases the

enthalpy and the GB energy are only affected to a small extent. The concentration of dimers ($\langle bp \rangle_{\%} \approx 3\%$) and the relative fraction of *donor–acceptor* energy [$\langle U_{\text{DA}}^* \rangle / \langle U^* \rangle \approx 3\%$] at $T^*/T_{\text{NI}}^* = 1$ show that the driving force of the N–I transition is still the Gay–Berne anisotropic interaction and no evident pre-transitional effects due to association are found. The DA energy does not alter considerably the thermodynamic and structural properties of the isotropic and nematic phases (see figure 7). The percentage of associated particles increases regularly decreasing the temperature but remains within $\approx 10\%$ down to $T^* = 1.2$, where the order parameter $\langle P_2 \rangle$ is already very high. The existence of a fraction of dimers in the nematic phase is detected by the radial distribution function

$$g_0(r^*) = \frac{1}{4\pi r^{*2} \rho^*} \langle \delta(r_{ij}^* - r^*) \rangle_{ij}, \quad (12)$$

and by the orientational correlation function

$$S^{110}(r^*) = -\frac{1}{3^{1/2} 4\pi r^{*2} \rho^*} \langle \delta(r_{ij}^* - r^*) \hat{\mathbf{u}}_i \cdot \hat{\mathbf{u}}_j \rangle_{ij}, \quad (13)$$

at $T^* = 1.25$ and $\langle P_2 \rangle = 0.79$ (figure 9, top plate) which show a small but sharp peak at $r^* \equiv r/\sigma_s \approx 2$, corresponding to the intermolecular distance for the associated configuration shown in figure 2.

On continuing to decrease the temperature, the percentage of *donor–acceptor* energy suddenly jumps to 20% in correspondence with a large scale association process and a second phase transition at $T^* \approx 1.15$. The structure of the fluid is dramatically altered and an intercalated highly ordered phase is formed with periodicity half the molecular length. Since the MC equilibration for this highly ordered phase is considerably difficult (even using *dimer* and *flip* moves), the detailed study of the associated system at these low temperatures has not been exhaustive. The temperature shift with respect to the nematic–smectic transition for the reference system is now quite high and a comparison of molecular organization snapshots at similar order parameter $\langle P_2 \rangle$ (figures 10 and 11) shows the principal differences between the SmA structure of the reference and that for the A_1 system (figure 11). The particles are shaded in dark gray if associated and in light gray otherwise. The *donor* and *acceptor* sites are represented as a black area on the particle’s surface at the molecule tip.

We now turn to the strong associating regime ($\epsilon_{\text{DA}}^+/\epsilon_0 = 10$) whose behaviour is considerably different from the reference system R. The N–I transition is shifted to higher temperatures ($T_{\text{NI}}^* \approx 1.75$), and the enthalpy versus temperature shows a considerable deviation from the reference one. The most striking feature is the trend in concentration of dimers $\langle bp \rangle_{\%}$ and of *donor–acceptor* energy [$\langle U_{\text{DA}}^* \rangle / \langle U^* \rangle$] $_{\%}$. Both curves

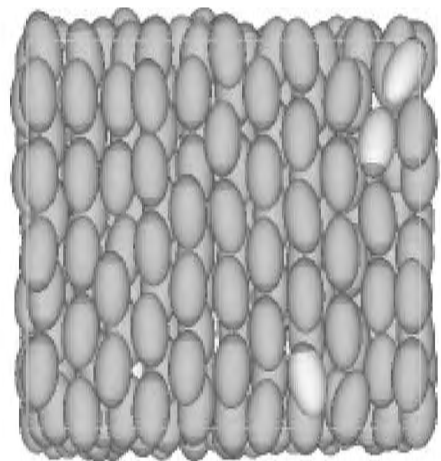
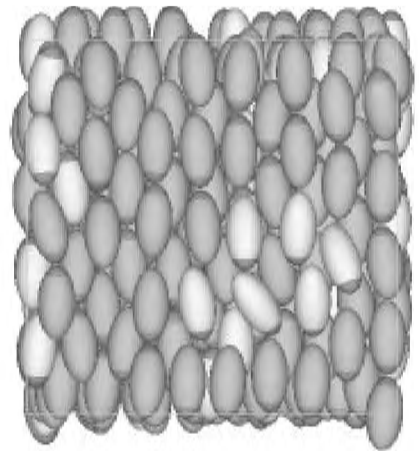
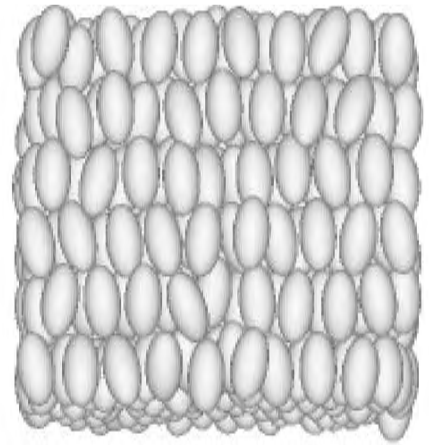
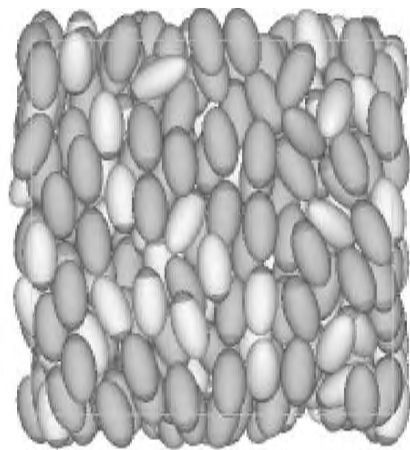
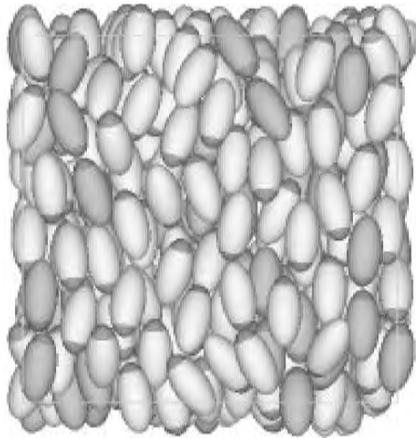
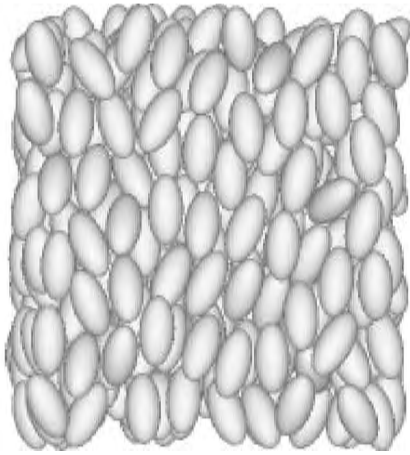


Figure 10. Snapshots of MC configurations of nematic phases with similar second rank order parameter $\langle P_2 \rangle$ for system R ($T^* = 1.15$, $\langle P_2 \rangle = 0.82$, top), system A₁ ($T^* = 1.20$, $\langle P_2 \rangle = 0.82$, centre) and system A₂ ($T^* = 1.60$, $\langle P_2 \rangle = 0.83$, bottom). The GB particles are represented in dark gray if associated and in light grey otherwise. The DA binding sites are indicated by the black tip. The MC configurations have been rotated in order to align the phase director with the vertical axis.

Figure 11. Snapshots of MC configurations of smectic phases with similar second rank order parameter $\langle P_2 \rangle$ for system R ($T^* = 1.00$, $\langle P_2 \rangle = 0.94$, top), system A₁ ($T^* = 1.10$, $\langle P_2 \rangle = 0.96$, centre) and system A₂ ($T^* = 1.45$, $\langle P_2 \rangle = 0.98$, bottom). The same colour coding described in figure 10 has been used. The MC configurations have been rotated in order to align the phase director with the vertical axis.

reveal that even in the isotropic phase a relevant fraction of particles are already associated and at $T^*/T_{NI}^* = 1$ almost 30% of the molecules are dimerized. For the strongly associating system A_2 the driving force of the N-I transition is the hydrogen bond interaction and considerable pre-transitional effects due to association are found. We notice that the percentage of bonded particles increases linearly when decreasing T^* and does not show significant jumps at the isotropic–nematic transition but grows until it becomes more than 70% when the DA interaction contributes to about 40% of the total energy. It is however interesting to see that the orientational properties of the nematic phase are not dramatically affected by the onset of dimerization and the plot of $\langle P_2 \rangle$ versus T^* is similar to the reference one. The profiles of the radial distribution function $g_0(r^*)$ and the orientational correlation $S^{110}(r^*)$ at $T^* = 1.65$ (figure 9, bottom plate) are consistently affected by the high fraction of dimers and the feature at $r^* \approx 2$ is extremely well defined.

Going to very low temperatures we see that once more there is not a sudden jump in the percentage of donor–acceptor energy as for system A_1 but that a limiting plateau is smoothly reached (figure 7, bottom). The association is almost complete and an intercalated highly ordered phase is again found. The temperature shift with respect to the smectic–nematic transition for the reference system is now higher than in the A_1 system. A graphical representation of the molecular organizations found for systems R, A_1 and A_2 at two selected temperatures with similar orientational order parameter $\langle P_2 \rangle$ are given in figures 10 and 11.

5. Conclusions

We have put forward a simple model for hydrogen-bonding Gay–Berne nematogens. We have considered relatively short rods (*length-to-breadth* ratio of $k = 2$) that only form ordered phases at very low temperatures and we have then shown that for sufficiently strong dimerizing interaction the nematic–isotropic transition temperature is raised by as much as 25%. The onset of nematic order from the isotropic phase shows a fairly different mechanism for the weak and strong associating systems. In the first case alignment is driven by the anisotropic interactions between monomers with a negligible fraction of dimers at the nematic transition. Conversely, ordering in the more strongly associating systems is assisted and favoured by the preliminary formation of a significant fraction of elongated dimers (about 30% at the isotropic–nematic transition). Both weak and strong associating systems form at low temperatures an intercalated smectic with a very different structure from that formed by the non-associating monomers. In summary, the present model seems

powerful enough to be of help in the understanding of the interplay of attractive, repulsive and associating anisotropic interactions and thus hopefully to contribute to a more rational employment of hydrogen bonded interactions in molecular design of novel liquid crystals.

We thank MURST *ex40%*, CNR *PF MSTA-II*, University of Bologna, EU TMR contract FMRX-CT97-0121 and NEDO for financial support.

References

- [1] GRAY, G. W., and JONES, B., 1953, *J. chem. Soc.*, 4179.
- [2] GRAY, G. W., 1962, *Molecular Structure and the Properties of Liquid Crystals* (London: Academic).
- [3] KATO, T., JIN, C., KANEUCHI, F., and URYU, T., 1993, *Bull. chem. Soc. Jpn.*, **66**, 3581.
- [4] KATO, T., JIN, C., KANEUCHI, F., URYU, T., and FRÉCHET, J. M. J., 1993, *Liq. Cryst.*, **14**, 1311.
- [5] KATO, T., and FRÉCHET, J. M. J., 1989, *J. Am. chem. Soc.*, **111**, 8533.
- [6] PRICE, D. J., WILLIS, K., RICHARDSON, T., UNGAR, G., and BRUCE, D. W., 1997, *J. mater. Chem.*, **7**, 883.
- [7] KIHARA, H., KATO, T., URYU, T., UJIE, S., KUMAR, U., FRÉCHET, J. M. J., BRUCE, D. W., and PRICE, D. J., 1996, *Liq. Cryst.*, **21**, 25.
- [8] TIAN, Y., XU, X., ZHAO, Y., TANG, X., and LI, T., 1997, *Liq. Cryst.*, **22**, 87.
- [9] WALLAGE, M. J., and IMRIE, C. T., 1997, *J. mater. Chem.*, **7**, 1163.
- [10] QIU, H. J., LI, M., CHEN, X. F., JING, F. Y., and ZHOU, E. L., 1998, *Liq. Cryst.*, **25**, 419.
- [11] AAKERÖY, C. B., and SEDDON, K. R., 1993, *Chem. Soc. Rev.*, 397.
- [12] KLEPPINGER, R., LILLYA, C. P., and YANG, C., 1997, *J. Am. chem. Soc.*, **119**, 4097.
- [13] FOUQUEY, C., LEHN, J. M., and LEVELUT, A. M., 1990, *Adv. Mater.*, **2**, 254.
- [14] ONSAGER, L., 1949, *Ann. New York Acad. Sci.*, **51**, 627.
- [15] SEAR, R. P., and JACKSON, G., 1994, *Molec. Phys.*, **82**, 473.
- [16] VEYTSMAN, B. A., 1995, *J. chem. Phys.*, **103**, 2237.
- [17] TROKHYMCHUK, A., PIZIO, O., HENDERSON, D., and SOKOLOWSKI, S., 1996, *Molec. Phys.*, **88**, 1491.
- [18] MCGROTHER, S. C., SEARS, R. P., and JACKSON, G., 1997, *J. chem. Phys.*, **106**, 7315.
- [19] GAY, J. G., and BERNE, B. J., 1981, *J. chem. Phys.*, **74**, 3316.
- [20] BERARDI, R., FAVA, C., and ZANNONI, C., 1995, *Chem. Phys. Lett.*, **236**, 462.
- [21] MOMANY, F., MCGUIRE, R., BURGESS, A., and SCHERAGA, H. J., 1975, *J. phys. Chem.*, **79**, 2361.
- [22] LIFSON, S., HAGLER, A. T., and DAUBER, P., 1979, *J. Am. chem. Soc.*, **101**, 5112, 5131.
- [23] HARVEY, S. C., PRABHAKARAN, M., and MCCAMMON, J. A., 1985, *Biopolymers*, **24**, 1169.
- [24] WEINER, S. J., KOLLMAN, P. A., CASE, D. A., SINGH, U. C., GHIO, C., ALAGONA, G., PROFETA JR, S., and WEINER, P., 1984, *J. Am. chem. Soc.*, **106**, 765.
- [25] LEVITT, M., and SHARON, R., 1988, *Proc. Nat. Acad. Sci. USA*, **85**, 7557.
- [26] TIRADO-RIVES, J., and JORGENSEN, W. L., 1990, *J. Am. chem. Soc.*, **112**, 2773.
- [27] VEDANI, A., and HUHTA, D. W., 1990, *J. Am. chem. Soc.*, **112**, 4759.

- [28] METROPOLIS, N., ROSENBLUTH, A. W., ROSENBLUTH, M. N., TELLER, A. H., and TELLER, E., 1953, *J. chem. Phys.*, **21**, 1087.
- [29] WÜ, D., CHANDLER, D., and SMITH, B., 1992, *J. phys. Chem.*, **96**, 4077.
- [30] ORKOULAS, G., and PANAGIOTOUPOULOS, A. Z., 1994, *J. chem. Phys.*, **101**, 1452.
- [31] FRENKEL, D., 1995, *Observation, Prediction and Simulation of Phase Transition in Complex Fluids*, NATO ASI Series, edited by M. Baus, L. F. Rull and J. P. Ryckaert (Dordrecht: Kluwer Academic Publishers).
- [32] FRENKEL, D., and SMIT, B., 1996, *Understanding Molecular Simulation: From Algorithms to Applications* (San Diego: Academic Press).
- [33] ALLEN, M. P., and TILDESLEY, D. J., 1987, *Computer Simulation of Liquids* (Oxford: Clarendon Press).
- [34] FRENKEL, D., 1990, *Computer Modeling of Fluids, Polymers and Solids*, NATO ASI Series, edited by C. R. A. Catlow *et al.* (Dordrecht: Kluwer Academic Publishers).
- [35] BERARDI, R., ORLANDI, S., and ZANNONI, C., 1996, *Chem. Phys. Lett.*, **261**, 363.
- [36] BERARDI, R., ORLANDI, S., and ZANNONI, C., 1997, *J. chem. Soc. Faraday Trans.*, **93**, 1493.
- [37] BERARDI, R., EMERSON, A. P. J., and ZANNONI, C., 1993, *J. chem. Soc. Faraday Trans.*, **89**, 4069.
- [38] ALKORTA, I., ROZAS, I., and ELGUERO, J., 1998, *Chem. Soc. Rev.*, **27**, 163.